Journal of Applied Electrochemistry (2007) 37:233–239
DOI 10.1007/s10800-006-9240-x

A nucleation and growth study of gold nanowires and nanotubes in polymeric membranes

R.J. GILLIAM[1,*], S.J. THORPE[1] and D.W. KIRK[2]
[1]*Department of Materials Science and Engineering, University of Toronto, 184 College Street, Rm. 140, Toronto, Ontario, Canada M5S 3E4*
[2]*Department of Chemical Engineering and Applied Chemistry, University of Toronto, 200 College Street, Rm. 246, Toronto, Ontario, Canada M5S 3E5*
*(*author for correspondence, fax: + 1-416-978-4155, e-mail: ryan.gilliam@utoronto.ca)*

Received 20 March 2006; accepted in revised form 12 September 2006

Key words: electroless deposition, nanotube, nanowire, nucleation and growth, template synthesis

Abstract

Through the use of a technique known as template synthesis, it has become possible to synthesize a variety of different materials in the form of nanowires or nanotubes. Dependent upon which type of template is used, either randomly or regularly dispersed nanowires or nanotubes with a wide variety of nanopore diameters and lengths can be created. In this experiment, gold nanowires and nanotubes have been synthesized with diameters of 30, 100, and 800 nm in polycarbonate membranes. The kinetics and characteristics of growth can be greatly altered, dependent upon what operational parameters are employed during deposition. This study looks at the different growth factors that need to be considered when employing the template synthesis approach. These factors include the final expected geometry, the distribution of nucleation sites, the grain size distribution, and the deposition rate.

1. Introduction

Over the past few decades nanomaterials have begun to play a role in almost every aspect of technology. In particular, gold nanotubes and nanowires have received considerable research focus due to their possible application in many areas such as catalysis, electronics, optoelectronics, photonics, information storage, gas storage, energy conversion, fluid transportation, drug release, and chemical and biological sensing [1–11].

As the potential uses for these nanostructured materials have increased over the past few decades, so have the number of synthesis processes. This study looks specifically at gold nanowires and nanotubes prepared through a technique known as template synthesis. Currently, there are many research groups using various types of template synthesis for nanostructure fabrication [12–17]. This technique involves the deposition, either electrolytic or electroless, of a material onto a membrane structure containing randomly, or regularly dispersed, uniform nanopores. The use of this method has been extended to materials such as metals, polymers, carbons and semiconductors [18–24]. Through varying the size of the nanopores within the membrane, the thickness of the membrane and the deposition kinetics, a wide variety of nanowire and nanotube geometries can be obtained. The deposition kinetics can be varied through changing the concentration of either the plating or reducing species, by altering the pH of the solution, by varying the deposition temperature or by altering the fluid mechanics of the system [25].

With the advent of these new technologies, comes a need to clearly define the growth mechanisms of these nanowires or nanotubes. Not only is their size important, but also their final geometry and microstructure. For this particular study, one of the most common forms of template synthesis that employs polycarbonate track-etched nanopore membranes was used [26, 27]. These membranes are commercially available and range in nanopore diameters from 10 nm up to 12 μm.

The objectives of this research were to determine the growth mechanisms involved in electroless deposition of gold and to determine what type of geometries and microstructures can be expected when using the template synthesis approach. In particular, the overall geometry, the distribution of nucleation sites, the grain size distribution and the deposition rate were examined. In characterizing the growth mechanisms taking place during the electroless deposition of gold, membranes containing 30, 100, and 800 nm size pores were used.

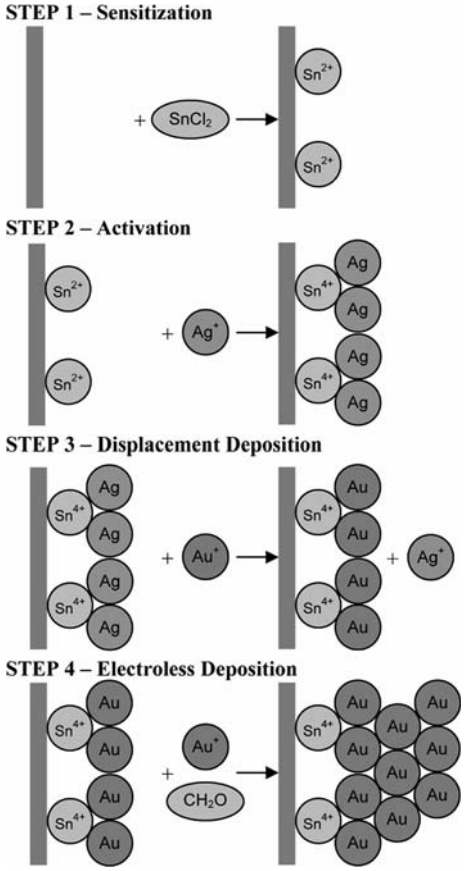

Fig. 1. Schematic diagram of four step electroless gold deposition on polycarbonate membranes. Adapted from Menon and Martin [26].

2. Experimental details

2.1. *Electroless deposition technique of gold nanowires and nanotubes*

2.1.1. *Membranes*

The membranes used for the following experiments were Nuclepore® track-etched polycarbonate membranes obtained from Whatman. These membranes are coated during manufacturing with a layer of polyvinylpyrrolidone in order to render the surfaces of the membranes hydrophilic. The polyvinylpyrrolidone also contains ion-complexing amine and carbonyl groups which act as molecular anchors during the deposition process [26]. Dependent upon the pore size of the membranes being used, the rated pore density can range from 10^6 to 10^8 pores cm^{-2}.

2.1.2. *Materials*

$SnCl_2$ (Fisher Scientific), CF_3COOH (Aldrich), CH_3OH (EMD), $AgNO_3$ (Engelhard), $NaHCO_3$ (BDH), Na_2SO_3 (Analar), and CH_2O (Aldrich) were all used as-received from the supplier. The gold plating solution used was a standard plating solution containing sodium gold sulphite ($Na_3Au(SO_3)_2$), which was obtained from Technic Inc. known as Oromerse Part B. The gold plating solution supplied was initially 0.3158 M, which was then diluted to achieve plating solutions of 3.85×10^{-3} M, 7.9×10^{-3} M (Industrial Standard) and 11.55×10^{-3} M. All solutions were made using 18 MΩ Type I water.

2.1.3. *Electroless gold deposition*

Apart from varying the Au concentration, pH, and temperature of the plating solutions all the membranes were subjected to the same general deposition procedure. Electroless deposition of gold was chosen as opposed to electrolytic deposition since electroless deposition allows for a slower, more uniform, deposit to be applied. Without this slower, more uniform deposition rate, it is not possible to obtain nanowires and nanotubes within the 30–100 nm range [26].

The electroless deposition chemistry employed in this study was adapted from work by Menon and Martin [26]. Based on prior deposition experience, an extra stabilizing component was added to the gold plating solution. The deposition of gold onto the membranes takes place in four steps. The first step, referred to as sensitization, consists of immersing the membrane in a 50 volume% methanol/water solution containing 0.026 M $SnCl_2$ and 0.07 M CF_3COOH. This results in the deposition of Sn^{2+} onto the entire membrane surface at the amine and carbonyl locations on the polyvinylpyrrolidone. The second step, referred to as the activation step, consists of immersing the membrane in a 0.029 M aqueous solution of ammonical $AgNO_3$. This results in a redox reaction taking place between the Sn and Ag, where the Sn is oxidized from Sn^{2+} to Sn^{4+}, and the Ag^+ is reduced to Ag. This produces a monolayer of Ag on the membrane surface. The third step, referred to as displacement deposition, consists of replacing the Ag on the membrane surface with Au. Since Au is a more noble metal then Ag, the Au^+ ions will displace the Ag on the surface, leaving Au and returning the Ag^+ to solution. This is done through immersing the membrane in a solution containing 0.0125 M $NaHCO_3$, 0.636 M Na_2SO_3 and diluted Oromerse B. At the same time 0.5 M of CH_2O was added to the solution in order to carry out the fourth step. The fourth step is the electroless deposition of gold. In this step, the gold coated surface acts as a catalytic site for the oxidation of formaldehyde and the subsequent reduction of Au^+ ions to elemental Au. This reaction is depicted below.

$$2Au^+ + CH_2O + 3OH^- \rightarrow HCOO^- + 2H_2O + 2Au\downarrow \quad (1)$$

In determining the nucleation distribution, the grain size distribution and the deposition rate, different operational parameters were varied; namely pH, temperature and Au concentration. To vary the bath pH 0.5 M H_2SO_4 or 1.0 M NaOH was used to decrease or increase the pH, respectively. The bath temperature was controlled using a refrigeration system and the Au concentration of the system was altered as mentioned previously. The four separate stages employed in the

electroless deposition of gold onto the polycarbonate membranes are depicted schematically in Figure 1.

After deposition was complete an Au coating was present over the entire surface of the membrane. In order to expose one surface so that the ends of the nanowires or nanotubes could be observed, one gold surface was removed simply by wiping the surface with a lab wipe while the membrane was still wet. The membrane was then placed in a 25 volume% nitric acid (HNO_3) solution for 12 h in order to remove residual Ag from the membrane.

In order to characterize the effects of these operational parameters on the nucleation distribution distance, grain size and the deposition rate, scanning electron microscopy (SEM), transmission electron microscopy (TEM), ultramicrotoming and image analysis software were used to analyse each sample.

2.2. *SEM, TEM, and image analysis measurements*

SEM was performed on either a Hitachi S-4500 or a Hitachi S-5200. To view the nanowires or nanotubes on the SEM the polycarbonate membrane had to be dissolved. The side of the membrane still coated in Au was carbon glued onto a piece of copper, leaving the uncoated surface exposed. This exposed side of the membrane was then subjected to ethylene chloride, or argon/oxygen plasma dependent upon the extent of removal required [28]. To view the tips of the nanowires or nanotubes, the membranes were placed in argon-10% oxygen plasma for 10–60 s. In order to remove the entire polycarbonate structure the membrane was exposed to ethylene chloride for 5 min.

TEM was performed either on a Hitachi HD-2000 (STEM) or an FEI Technai 20 (TEM). To view the length profile of the nanowires or nanotubes, both surfaces of the membrane were removed using lab wipes as described above, and then the membrane was dissolved completely in ethylene chloride. Drops of this dissolved solution were then placed onto formvar-carbon coated copper grids. To view the cross-sections of the nanowires or nanotubes ultramicrotoming was used. Each sample was ultramicrotomed at room temperature into 50 nm slices and these slices were collected onto TEM grids.

In order to characterize the thickness of the gold deposition with respect to time, the distribution of grain sizes and the density of the membranes, a LECO IA-3001 Image Analysis System was used.

3. Results and discussion

To use Au nanowires or nanotubes for any of the applications outlined it is important to be able to predict and control the final geometry and microstructure. The final shape expected, the final wall thickness and the final microstructure will all play an important role dependent upon what application is being employed.

3.1. *General geometry*

Membranes, as received from the manufacturer, were viewed using SEM to analyse average pore size and distribution. As seen in Figure 2, for a given pore diameter, the pores are relatively standard in size (+0% to −20% as specified by the manufacturer), and randomly distributed.

After performing electroless deposition, the membranes were dissolved using ethylene chloride so that the entire nanowires or nanotubes could be analysed using TEM. As seen in Figure 3, the outside diameters of the nanowires or nanotubes are not constant. Instead, they are scalloped in shape, varying in diameter along the lengthwise cross-section of the structure. The diameters at each end of the nanostructure are smaller compared to the diameter at the centre of the nanostructure. This is a direct result of the manufacturing of the membranes, and is more pronounced for the smaller pore diameters.

The final geometric consideration is the wall thickness obtained during the electroless deposition procedure. The wall thickness is in direct correlation to the diffusion behaviour exhibited by the Au^+ ions and is not uniform over the entire length of the nanopores. Instead, there is a higher deposition rate of Au near the exterior surface of the membrane, resulting in thicker

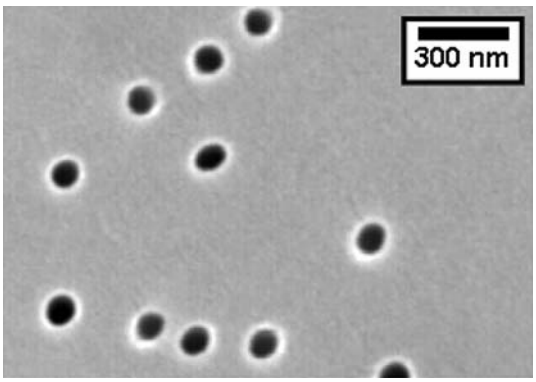

Fig. 2. Track-etched polycarbonate membranes containing 100 nm pores as received from manufacturer.

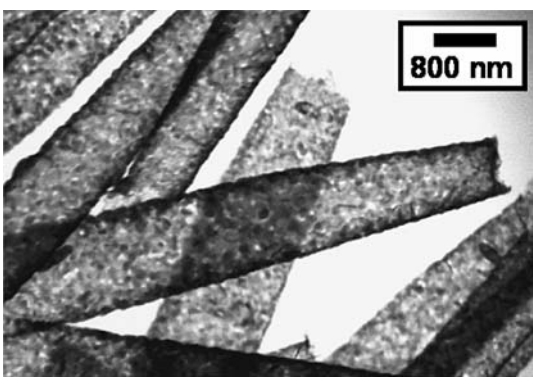

Fig. 3. TEM image showing scalloped nature exhibited by nanowires and nanotubes.

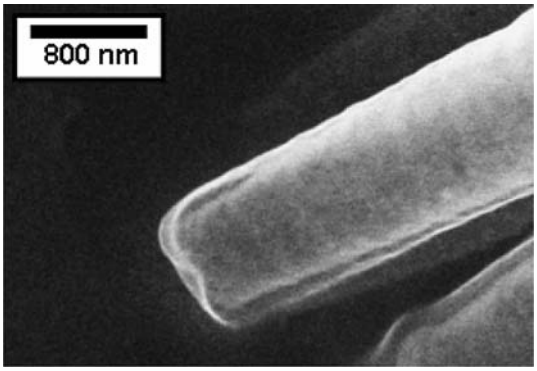

Fig. 4. SEM image exhibiting non-uniform wall thickness near the end of the nanotube.

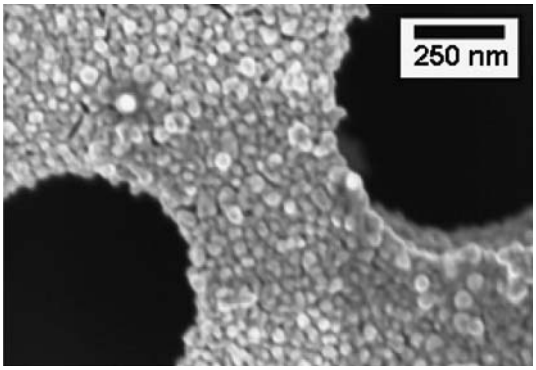

Fig. 5. Example of gold nucleation distribution distance on the surface of an 800 nm pore size membrane (60 min deposition time).

walls at each entrance to the pore. The consequence of this phenomenon can be seen in Figure 4.

3.2. *Nucleation site distribution*

Using the procedure outlined in the experimental section, gold electroless deposition was carried out for time intervals of 20, 40, 60 and 90 min on 30, 100 and 800 nm samples. To determine the effect of pH, temperature and Au concentration on the nucleation site distribution distance, each of these parameters was varied independently with respect to a standard industrial solution (pH of 10, temperature of 1 °C, $[Au^+]$ of 7.9×10^{-3} M). The gold coated surfaces of each membrane, both within the nanopores and on the top and bottom, were then viewed under SEM. In addition, microtomed and lengthwise samples were viewed under TEM.

In looking at the distribution of nucleation sites with respect to each of these samples, two interesting phenomena were observed. First, after only 20 min of deposition, the membranes were covered with small, separate clusters of gold. From this, it can be concluded that once displacement deposition has occurred at a site between Au and Ag, then step 3 and step 4 of the process begin to compete. These initial nucleation sites act as catalysts for the oxidation of formaldehyde allowing for further deposition onto these sites. These initial nucleation sites continue to grow as separate islands until eventually the gold islands grow into one another. The spacing between these initial nucleation sites, which is represented by the size of these islands after they have grown into one another, is termed the nucleation distribution distance. An example of gold islands covering the surface of a membrane is depicted in Figure 5.

To compare the nucleation distribution distance on the surface of the membranes to that within the nanopores, microtomed cross-sections of the gold deposit were analysed. Figure 6 depicts a microtomed cross-section of a nanopore and surface.

Image analysis software was used to calculate the nucleation distribution distance both within the nanpores and on the surface of the membrane. Through analyzing both Figure 6a and b, it was found that for a given set of deposition parameters, the nucleation distribution distance is relatively uniform over all surfaces of the membrane, both inside the nanopores and on the surface of the membrane. These results are depicted in Figure 7.

Second, it was found that for a given set of deposition parameters (pH, temperature and Au concentration), there exists a characteristic nucleation distribution distance. For the standard industrial plating solution (pH of 10, temperature of 1 °C, $[Au^+]$ of 7.9×10^{-3} M), this characteristic nucleation distance was roughly 30 nm, and is represented in both Figures 5 and 6.

To determine the individual effect of pH, temperature and Au concentration on this characteristic nucleation distribution distance, each of these parameters were varied independently with respect to the standard industrial solution. Au concentrations of 3.85×10^{-3} M, 7.9×10^{-3} M, and 11.55×10^{-3} M, pH of 6, 8, and 10, and temperatures of 1 and 25 °C were used. Using image analysis software, the average nucleation distribution distance was calculated for each sample. Results are given in Figure 8.

As seen from Figure 8, with an increase in Au concentration there was an increase in the characteristic nucleation distribution distance. As Au concentration was increased, the deposition rate of the system also increased. As the pH of the system increased in the basic region, there was an increase in the characteristic nucleation distribution distance and the deposition rate. As expected from the electroless deposition formula, for pH values in the acidic range, no electroless deposition of gold occurred on the membrane surface. With increase in temperature, again there was an increase in the characteristic nucleation distribution distance as well as the deposition rate. In all three cases an increase in deposition rate increased the characteristic nucleation distance. This increase in deposition rate caused step 4 of the procedure to proceed more readily then step 3, driving the growth of nucleated sites as opposed to further nucleation.

This ability to tailor the nucleation distribution distance makes it possible to achieve smaller diameter

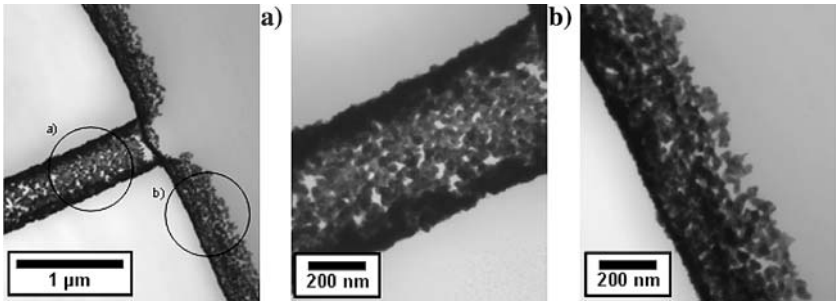

Fig. 6. Microtomed cross-section of an 800 nm pore size sample (4 h deposition time) depicting the nucleation distribution distance both; (a) within the nanopores, and (b) on the surface of the membrane.

nanowires and thinner walled nanotubes. For nanowires, to achieve a continuous deposit through the entire nanopores, it is important to have a nucleation distribution distance less then the size of the nanopores. Otherwise, nucleation and growth will lead to blockage of the nanopores. Likewise, to achieve a continuous wall structure for a nanotube, it is important to have a nucleation distribution distance less then the desired wall thickness. Otherwise, nucleation and growth will lead to a discontinuous wall structure. An example of continuous 30 nm nanowires is shown in Figure 9.

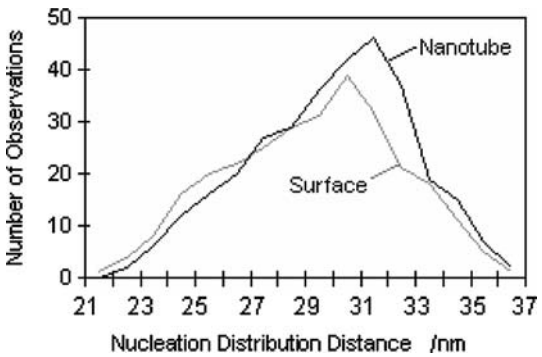

Fig. 7. Comparison of the nucleation distribution distance on the nanotube wall to that on the surface of the membrane (4 h deposition time).

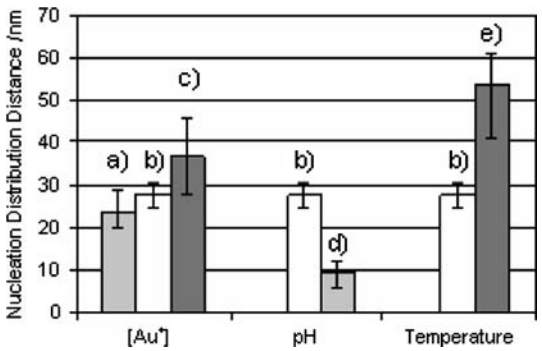

Fig. 8. Effect of independently varying the Au concentration, pH, and temperature on nucleation distribution distance. Parameters were varied relative to (b), the standard industrial electroless deposition bath (pH of 10, temperature of 1 °C, $[Au^+]$ of 7.9×10^{-3} M); (a) $[Au^+]$ of 3.85×10^{-3} M; (c) $[Au^+]$ of 11.55×10^{-3} M; (d) pH of 8; (e) temperature of 25 °C.

3.3. *Grain size distribution*

In looking at the grain sizes produced during deposition, 800 nm pore size samples were analysed at deposition times of 2, 4, 6, 8, 10, 12 and 24 h. At lower deposition times, it was found that the characteristic nucleation distance which was initially established during deposition continued into the samples as electroless deposition continued. However, at longer deposition times, the grain size changed from a uniformly sized structure to a tri-modal structure. Using image analysis software, it was seen that for an 800 nm pore size sample, subjected to 24 h of electroless deposition in the standard industrial bath outlined earlier, three separate grain sizes became prominent. Similarly to the samples that underwent deposition for shorter periods of time, there were grains in the 30 nm range. There were also grains in the 75 nm range and grains in the 200 nm range. A sample illustrating this tri-modal grain structure is depicted in Figure 10. The distribution of grains is depicted in Figure 11.

The reason for this tri-modal structure is related to a change in deposition rate with respect to time. In performing electroless deposition on these membrane structures, a batch system was employed. As time progressed, both the Au concentration and pH

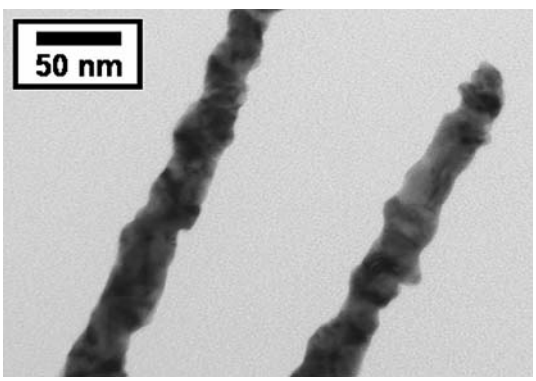

Fig. 9. Example of continuous 30 nm nanowires (60 min deposition time).

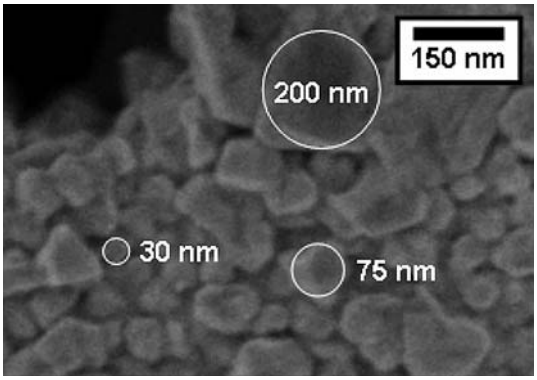

Fig. 10. 800 nm pore size sample illustrating tri-modal grain size distribution.

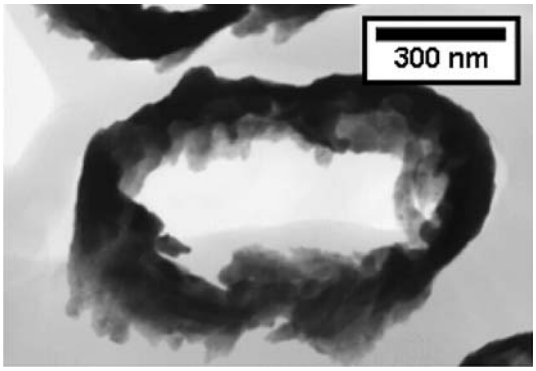

Fig. 12. Cross-section of an 800 nm pore size sample subjected to 4 h of deposition.

decreased, leading to a change in deposition kinetics. It was found that when a continuous bath set-up was employed, where the pH and Au concentration were kept constant, the grain size continued to reflect that of the characteristic nucleation distance. This indicates that the grain size of the gold deposit is a direct function of the deposition parameters and not the deposition time. To develop a clearer understanding of which deposition parameters are governing the grain size distribution more work needs to be carried out.

3.4. *Deposition rate*

In performing electroless deposition of Au onto the polycarbonate membranes, a plating solution of 40 ml was used for each case. Within this solution there is a finite amount of Au^+ present, which decreases over time as the Au^+ plates onto the membrane surface. This change of concentration over time has an impact on the diffusion properties of the solution, and a subsequent impact on the deposition rate.

In developing a correlation between tube wall thickness and time, samples were analysed at 60, 90, 120, 240, 360 and 1200 min. These samples were each microtomed and viewed under TEM to analyse their cross section. Using image analysis software, a direct measurement of the wall thickness with respect to time was obtained. An example of a microtomed sample is depicted in Figure 12, and the thickness profile with respect to deposition time in Figure 13.

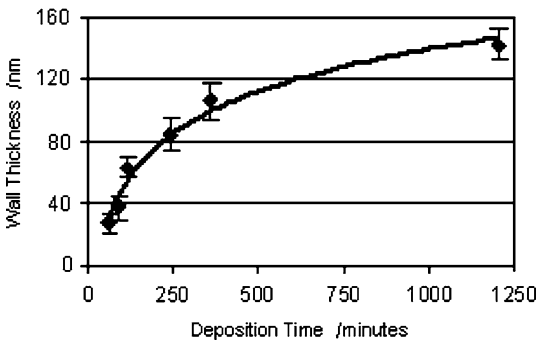

Fig. 13. Thickness of nanotube walls with respect to time for 800 nm pore size samples.

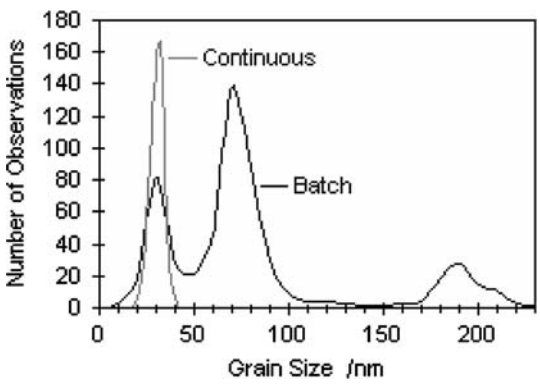

Fig. 11. Tri-modal grain size distribution of 800 nm pore size sample depicted in Figure 10.

It can be seen that there is a decrease in the deposition rate with time. This impact is due to both a change in concentration with time and a change in the diffusion kinetics. Aside from concentration, pH also plays a role. From previous experiments, it was found that with a decrease in pH, there is a decrease in deposition rate. As can be seen from the redox equation step 4, as deposition continues, the solution pH continues to decrease, further contributing to the decrease in overall deposition rate with time. In developing a diffusion model for this system, concentration, pH and pore diameter all need to be incorporated.

4. Conclusion

Through the use of the template synthesis approach it was found that gold nanowires and nanotubes can easily, and reproducibly be made within defined geometric constraints.

Based on the operational parameters employed, a characteristic nucleation site distribution and grain size can be obtained. Through varying the deposition operational parameters these distribution distances can be precisely controlled. This ability to tailor nucleation

distances enables the production of smaller diameter nanowires and thinner walled nanotubes.

Acknowledgements

This work was supported through the Ontario Graduate Scholarship for Science and Technology (OGSST) as well as the University of Toronto Materials Engineering Open Fellowship.

References

1. M. Wirtz and C.R. Martin, *Adv. Mater* **15**(5) (2003) 455.
2. R.E. Gyurcsányi, T. Vigassy and E. Pretsch, *Chem. Commun.* (2003) 2560.
3. D.T. Mitchell, S.B. Lee, L. Trofin, N. Li, T.K. Nevanen, H. Söderlund and C.R. Martin, *J. Am. Chem. Soc* **124** (2002) 11864.
4. Y. Kobayashi and C.R. Martin, *Anal. Chem* **71** (1999) 3665.
5. P. Ugo, L.M. Moretto, S. Bellomi, V.P. Menon and C.R. Martin, *Anal. Chem* **68**(23) (1996) 4160.
6. M. Nishizawa, V.P. Menon and C.R. Martin, *Science* **268** (1995) 700.
7. C.G. Zoski, *Electroanalysis* **14** (2002) 1041.
8. Y. Sun and Y. Xia, *Adv. Mater* **16**(3) (2004) 264.
9. Y. Sun, B. Wiley, Z.Y. Li and Y. Xia, *J. Am. Chem. Soc* **126** (2004) 9399.
10. E. Finot, R. Bourillot, R. Meunier-Prest, Y. Lacroute, G. Legay, M. Cherkaoui-Malki, N. Latruffe, O. Siri, P. Braunstein and A. Dereux, *Ultramicroscopy* **97** (2003) 441.
11. T. Uematsu, L. Fan, T. Maruyama, N. Ichikuni and S. Shimazu, *J. Mol. Catal. A: Chem* **182–183** (2002) 209.
12. C.R. Martin, *Science* **266** (1994) 1961.
13. P. Forrer, F. Schlottig, H. Siegenthaler and M. Textor, *J. Appl. Electrochem.* **30** (2000) 533.
14. N. Li, S. Yu, C. Harrell and C.R. Martin, *Anal. Chem* **76** (2004) 2025.
15. A. Stein, *Microporous Mesoporous Mater* **44–45** (2001) 227.
16. Y. Xia, P. Yang, Y. Sun, Y. Wu, B. Mayers, B. Gates, Y. Yin, F. Kim and H. Yan, *Adv. Mater* **15**(5) (2003) 353.
17. L. Xu, L.D. Tung, L. Spinu, A.A. Zakhidov, R.H. Baughman and J.B. Wiley, *Adv. Mater* **15**(18) (2003) 1562.
18. C.R. Martin, L.S. Van Dyke, Z. Cai and W Liang, *J. Am. Chem. Soc* **112** (1990) 8976.
19. L.S. Van Dyke and C.R. Martin, *Langmuir* **6** (1990) 1118.
20. S.A. Sapp, D.T. Mitchell and C.R. Martin, *Chem. Mater* **11** (1999) 1183.
21. B.B. Lakshmi, P.K. Dorhout and C.R. Martin, *Chem. Mater* **9** (1997) 857.
22. S.A. Miller, V.Y. Young and C.R Martin, *J. Am. Chem. Soc* **123** (2001) 12335.
23. C.J. Patrissi and C.R. Martin, *J. Electrochem. Soc* **148** (2001) A1247.
24. K Yamada, R Gasparac and C.R. Martin, *J. Electrochem. Soc* **151**(1) (2004) E14.
25. T. Watanabe, *Nano-Plating: Microstructure Control Theory of Plated Film and Data Base of Plated Film Microstructure* (Elsevier Ltd, Oxford, 2004).
26. V.P. Menon and C.R. Martin, *Anal. Chem.* **67** (1995) 1920.
27. M. Wirtz, M. Parker, W. Kobayashi and C.R Martin, *Chem. Eur. J.* **8**(16) (2002) 3572.
28. S. Yu, N. Li, J. Warton and C.R. Martin, *Nano Lett* **3**(6) (2003) 815.